STEM CELLS®

TISSUE-SPECIFIC STEM CELLS

Migration of Neurotrophic Factors-Secreting Mesenchymal Stem Cells Toward a Quinolinic Acid Lesion as Viewed by Magnetic Resonance Imaging

OFER SADAN,[a] NOAM SHEMESH,[b] RAN BARZILAY,[a] MERAV BAHAT-STROMZA,[a] ELDAD MELAMED,[a] YORAM COHEN,[b] DANIEL OFFEN[a]

[a]Laboratory of Neurosciences, Felsenstein Medical Research Center, Department of Neurology, Rabin Medical Center, Sackler Faculty of Medicine, and [b]School of Chemistry, The Raymond and Beverly Sackler Faculty of Exact Sciences, Tel Aviv University, Tel Aviv, Israel

Key Words. Quinolinic acid • Huntington's disease • Mesenchymal stem cells • Cell migration • Neurotrophic factors • Cellular magnetic resonance imaging • Cell tracking

ABSTRACT

Stem cell-based treatment is a promising frontier for neurodegenerative diseases. We propose a novel protocol for inducing the differentiation of rat mesenchymal stem cells (MSCs) toward neurotrophic factor (NTF)-secreting cells as a possible neuroprotective agent. One of the major caveats of stem cell transplantation is their fate post-transplantation. To test the viability of the cells, we tracked the transplanted cells in vivo by magnetic resonance imaging (MRI) scans and validated the results by histology. MSCs went through a two-step medium-based differentiation protocol, followed by in vitro characterization using immunocytochemistry and immunoblotting analysis of the cell media. We examined the migratory properties of the cells in the quinolinic acid (QA)-induced striatal lesion model for Huntington's disease. The induced cells were labeled and transplanted posterior to the lesion. Rats underwent serial MRI scans to detect cell migration in vivo. On the 19th day, animals were sacrificed, and their brains were removed for immunostaining. Rat MSCs postinduction exhibited both neuronal and astrocyte markers, as well as production and secretion of NTFs. High-resolution two-dimensional and three-dimensional magnetic resonance images revealed that the cells migrated along a distinct route toward the lesion. The in vivo MRI results were validated by the histological study, which demonstrated that phagocytosis had only partially occurred and that MRI could correctly depict the status of the migrating cells. The results show that these cells migrated toward a QA lesion and therefore survived for 19 days post-transplantation. This gives hope for future research harnessing these cells for treating neurodegenerative diseases. STEM CELLS *2008;26:2542–2551*

Disclosure of potential conflicts of interest is found at the end of this article.

INTRODUCTION

Stem cell-based therapy for neurodegenerative diseases has been widely investigated in two main directions: cell replacement and tissue support. The first approach aims at replacing the degenerated neurons. The second approach claims that stem cells might provide a better environment for damaged tissue and save the remaining neurons. The objective is to fight the common pathway of the neurodegenerative processes exhibited in many of these diseases, such as excitotoxicity, oxidative stress, and so forth. The trophic effect in the impaired tissue may be provided by cells that secrete neurotrophic factors (NTFs) [1].

Huntington's disease (HD) is an autosomal dominant inherited disease that is clinically manifested by involuntary choreiformic (dance-like) movements, emotional instability, and dementia. Increased amounts of quinolinic acid (QA), a tryptophan endogenous metabolite, are found in the striatum of HD patients at the early stages of the disease and also in the striatum and cortex of several transgenic mice models of the disease [2, 3]. When injected into the rat striatum, QA induces a striatal lesion that resembles the microscopic pathology viewed in HD patients: namely, a specific loss of medium spiny neurons (mostly GABAergic) and sparing of dopaminergic and cholinergic neurons and axonal damage, due to excitotoxicity [4].

Mesenchymal stem cells (MSCs) are a distinct population of cells in the bone marrow that have the potential to differentiate into bone, cartilage, and fat tissues [5]. These cells are considered as candidates for neurodegeneration therapeutics since they express neural markers at their basal level, a fact that probably contributes to their neural-like differentiation capabilities [6]. Two advantages of MSCs are that they can be easily obtained

Author contributions: O.S. and N.S.: conception and design, collection and assembly of data, data analysis and interpretation, manuscript writing; O.S. and N.S. contributed equally to this work; R.B. and M.B.-S.: collection and assembly of data, data analysis and interpretation; E.M., Y.C., and D.O.: conception and design, financial support, final approval of the manuscript.

Correspondence: Daniel Offen, Ph.D., Neurosciences Laboratory, Felsenstein Medical Research Center, Rabin Medical Center, Petah Tikva 49100, Israel. Telephone: 972-3-9376130; Fax: 972-3-9376130; e-mail: doffen@post.tau.ac.il; or Yoram Cohen, Ph.D., School of Chemistry, The Raymond and Beverly Sackler Faculty of Exact Sciences, Tel Aviv University, Ramat Aviv, Tel Aviv 69978, Israel. Telephone: 972-3-6407232; Fax: 972-3-6407469; e-mail: ycohen@post.tau.ac.il Received March 11, 2008; accepted for publication July 7, 2008; first published online in STEM CELLS *EXPRESS* July 17, 2008. 1066-5099/2008/$30.00/0 doi: 10.1634/stemcells.2008-0240

and autotransplanted. To date, MSCs have been transplanted as treatment in various animal models of neurodegenerative disorders, such as Parkinson's disease [7], multiple sclerosis [8], and stroke [9]. These cells possess several additional qualities, such as immunomodulation and immunosuppression on their surroundings [10]. Moreover, they react to several chemotactic signals, displaying homing capabilities [11].

In our laboratory, we developed a protocol for inducing bone marrow-derived MSCs into cells that express mainly astrocytic but also neuronal markers and secrete NTFs. In this study, these cells are used as part of our attempt to follow the tissue support and neuroprotection strategy. One of the main drawbacks in stem cell research is the lack of information regarding the fate of the transplanted cells in the host tissue [12–14]. As the stem cells are transplanted, they may encounter numerous obstacles that may limit their survival, ranging from the immune response to possible death by lack of nutrients and tissue stress. Another important determinant is the ability of the cells to migrate toward the damaged areas. Therefore, we decided to use magnetic resonance imaging (MRI) as a noninvasive and efficient method of determining the fate of the transplanted cells.

MRI is the most important imaging modality for studying central nervous system (CNS) disorders in a noninvasive manner. The high spatial resolution of MRI, coupled to its ability to portray diverse anatomical features of the brain by various contrast mechanisms, has made it the most suitable imaging modality for studying the CNS and diagnosing its disorders. However, due to the inherent low sensitivity and limited specificity of MRI, it is difficult to delineate transplanted cells from a host tissue without the use of contrast agents [15, 16]. The use of contrast agents has been shown to increase the sensitivity of MRI up to single-cell detection when micrometer-sized magnetic particles were used as contrast agents [17, 18].

Cell migration occurs in the CNS in developmental neurogenesis processes and also in the adult brain. Neural progenitors have been shown to express chemokine receptors and react to chemotactic stimuli in mouse embryo and mature brain [19]. Neurodegeneration induces changes in the migration capacity of progenitor cells [20]. In particular, an increase in migration was demonstrated in the QA-induced striatal lesion model of HD [21, 22]. Moreover, the upregulation of migration was shown under the influence of brain-derived neurotrophic factor (BDNF) [23]. The migration phenomena are now harnessed in the stem cell research field, especially in the MRI context, and there are accumulating data that demonstrate how exogenous stem cells of various origins migrate in the CNS [7, 8, 24], and specifically toward QA-induced lesion [25].

Histology-based studies provide end-point snapshots of the cells in the transplanted tissues. The advantage of in vivo imaging studies over end-point histology is that they enable longitudinal studies simultaneously demonstrating the progression of the pathology and the migratory capabilities of the stem cells [26]. By combining these two methodologies, we can deduce the migration properties and, consequently, the viability of the transplanted cells.

In the current study, we demonstrated autologous transplantation of rat MSCs following in vitro induction that upregulated production and secretion of NTFs. Furthermore, we transplanted superparamagnetic iron oxide (SPIO)-labeled induced cells into the brains of QA-lesioned rats, followed them in vivo using time-course high-resolution magnetic resonance (MR) images, and found that they survived and migrated toward the lesion. Finally, we assessed the histological pertinence to MR images and quantified the number of cells phaged by the host immune system.

Materials and Methods

Induction Protocol of Neurotrophic Factor-Producing Cells

MSCs were replaced with step 1 medium containing Dulbecco's modified Eagle's medium (DMEM) supplemented with 100 mg/ml streptomycin, 100 U/ml penicillin, 12.5 units/ml nystatin (SPN, Biological Industries, Beit Haemek, Israel, http://www.bioind.com), 2 mM L-glutamine (Biological Industries), 20 ng/ml human epidermal growth factor (R&D Systems Inc., Minneapolis, http://www.rndsystems.com), 20 ng/ml human basic fibroblast growth factor (hbFGF) (R&D Systems), and 10 μl/ml N2 supplement (5 μg/ml insulin, 20 nM progesterone, 100 μM putrescine, 30 nM selenium, 100 μg/ml transferrin [Invitrogen, Carlsbad, CA, http://www.invitrogen.com]). After 72 hours in the step 1 medium, cells were placed in step 2 medium, which consisted of DMEM supplemented with SPN, 2 mM L-glutamine, 1 mM Dibutyryl cyclic AMP (Sigma-Aldrich, St. Louis, http://www.sigmaaldrich.com), 0.5 mM 3-isobutyl-1-methylxanthine, 20 ng/ml hbFGF, 50 ng/ml human neuregulin1-β1 (R&D Systems), and 5 ng/ml platelet-derived growth factor-AA (PDGF; Peprotech, Rocky Hill, NJ, http://www.peprotech.com). As a control we used untreated MSCs that were grown in a serum-free medium containing DMEM, glutamine, and SPN.

Immunocytochemistry

Cells grown on coverslips were fixed with 4% paraformaldehyde for 10 minutes, washed with phosphate-buffered saline (PBS), and then incubated in a blocking and permeabilization solution (5% normal goat serum, 1% bovine serum albumin, and 0.5% Triton X-100 in PBS) and incubated with a primary antibody overnight at 4°C. After being washed with PBS, cells were incubated with either biotinylated secondary antibody or an Alexa-conjugated secondary antibody. Samples incubated with biotinylated antibody were further incubated for 1 hour at room temperature (RT, 20°C) with streptavidin conjugated to an Alexa fluorophore. The nuclei were counterstained with 4,6-diamidino-2-phenylindole (DAPI; 1:500; Sigma-Aldrich). The following primary antibodies were used (asterisk [*] indicates that the secondary antibody used was biotinylated): rabbit α-glial fibrillary acidic protein (GFAP; 1:200; Dako, Glostrup, Denmark, http://www.dako.com), rabbit α-BDNF (1:100*; Santa Cruz Biotechnology Inc., Santa Cruz, CA, http://www.scbt.com), mouse α-S100β (1:100; Sigma-Aldrich), rabbit α-vasculoendothelial growth factor (VEGF; 1:100*; Santa Cruz Biotechnology), mouse α-anti-β-tubulin III (1:1,000*; Sigma-Aldrich), rabbit α-glial-derived neurotrophic factor (GDNF; 1:100*; Santa Cruz Biotechnology), rabbit α-nerve growth factor (NGF; 1:100*; Santa Cruz Biotechnology), and rabbit α-glutamine synthetase (GS; 1:200; Sigma-Aldrich). Secondary antibodies were biotin-conjugated goat α-mouse IgG (ready-to-use; Zymed, Invitrogen), biotin goat α-rabbit IgG (1:200; Invitrogen), streptavidin-Alexa Fluor 488 (1:200; Invitrogen), and streptavidin-Alexa Fluor 568 (1:200; Invitrogen). The quantification of positive cells was performed on five random fields photographed at a magnification of $\times$200, as a percentage of the positive cells from the number of total DAPI-positive nuclei.

Western Blot Analysis

Cell supernatant postdifferentiation was collected, frozen, and quantified. The supernatant was concentrated using Centricon Centrifugal Filter Units (Millipore, Billerica, MA, http://www.millipore.com) to 5%–10% of the original volume, filtering out any substance lighter than 10 kiloDalton (kDa). Fifty microliters of each sample was separated by 12% SDS-polyacrylamide gel electrophoresis gels and transferred to a nitrocellulose membrane. The membranes were blocked in 5% nonfat milk for 1 hour at RT, incubated overnight at 4°C with a primary antibody followed by horseradish peroxidase-conjugated secondary antibody (1:10,000; Sigma-Aldrich), and developed with the ECL Plus detection system (GE Healthcare, Uppsala, Sweden, http://www.gelifesciences.com).

Cell Proliferation Assay

We used the 5-bromo-2′-deoxyuridine (BrdU) cell proliferation assay (Chemicon, Temecula, CA, http://www.chemicon.com) to compare the proliferation rate of the rat MSCs versus the induced MSCs. This enzyme-linked immunosorbent assay (ELISA) kit quantitates detection of newly synthesized DNA of actively proliferating cells. The assay was conducted according to the manufacturer's protocol in quadruplet, and results were read at wavelengths of 450/550 using an ELISA reader (Powerwave X; Biotek Instruments, Winooski, VT, http://www.biotek.com). The sum of the two controls (cells without BrdU exposure, and growth medium with BrdU exposure but without cells, measured in triplicate) was deducted from the average results. Results were normalized to the untreated MSCs.

Quinolinic Acid-Induced Striatal Lesion

Male Wistar rats ($n = 12$; Harlan, Jerusalem, http://www.harlan.com) weighing 230–250 g were used. They were placed under 12-hour-light/12-hour-dark conditions and grown in individually ventilated cages (IVC) with ad libitum access to food and water. All experimental protocols were approved by the University Committee of Animal Use for Research and Education. Every effort was taken to reduce the number of animals used and to minimize their suffering.

QA (Sigma-Aldrich) was dissolved in 1 M NaOH solution and then titrated with phosphate buffer to pH 7–7.4. Using a stereotactic frame under chloral hydrate anesthesia, 250 nmol was injected in 1 μl. The injection was aimed to the left midstriatum according to the rat brain atlas [27] at the following coordinates (relative to the bregma and dura): anterior, +0.7 mm; lateral, +2.7 mm; ventral, −4.8 mm. The injection rate was 0.5 μl/minute, and the inserted needle was withdrawn after 5 minutes.

Stem Cell Transplantation

Rat MSCs were labeled using the PKH26 fluorescent dye (Sigma-Aldrich) according to the manufacturer's protocol. A day after labeling, the cells underwent the induction protocol as described above. On the last day of step 1 medium, cells were labeled with SPIOs as previously described, with slight variations [28]. SPIOs (5 μg/ml; Feridex; Bayer HealthCare, Leverkusen, Germany, http://www.berleximaging.com) were incubated with poly-L-lysine (1 μg/ml medium; 70–150 kDa; Sigma-Aldrich) for 1 hour before adding SPIOs to the medium. Cultures were washed with the step 2 medium after 24 hours. On the last day, the treated cells were trypsinized, counted, and resuspended in PBS. Immediately after receiving QA, 250,000 cells were transplanted posterior to the lesion in the ipsilateral hemisphere (anterior, −4.7 mm; lateral, +2.7 mm; ventral, −5 mm). The injection was performed as described for the QA lesion above.

The experiment consisted of three treatment groups. The first control group was treated with QA as described, and instead of a cellular treatment, only SPIOs were injected to the same location as the stem cell transplantation ($n = 3$). The second control group was treated with PBS instead of QA, and the cells were transplanted as described above ($n = 3$). The last group was treated with both QA and cell transplantation ($n = 6$). The group treated with SPIOs only received 5 μg of Feridex in 1 μl of PBS. This dose was approximately the same as the dose to which 250,000 cells were exposed in the medium, but it was not necessarily the same as the intracellular incorporated amount of SPIOs.

MRI

Anesthesia was induced with 4% isoflurane in 95% O_2 and maintained with ~1%–2% isoflurane (Vetmarket Ltd., Petah Tikva, Israel) at a flow rate of ~1 l/minute. Respiratory rate was monitored throughout the entire set of experiments. Body temperature was maintained by circulating water at 37°C. MRI scans were performed on a 7.0-tesla (T)/30-cm Bruker Biospec (Bruker Biospin, Karlsruhe, Germany, http://www.bruker-biospin.com) equipped with a gradient system capable of producing gradient pulses of up to 400 mT/m. A body coil was used as the transmit coil, and a rat quadurature coil was used as the receiving coil. MRI experiments were performed on the day of the treatment (day 0) and 3, 8, and 18 days post-transplantation and QA injection. Scans included two-dimensional (2D) gradient echo (GE) images (fast low angle shot [FLASH], Repetition time/echo time [TR/TE] = 750/20 milliseconds, flip angle = 30°) and T_2 weighted images (WI) RARE8 (TR/TE = 3,500/75 milliseconds). For both scans, the field of view (FOV) was 2.56 × 2.56, the matrix size was 256 × 128 zero-filled to 256 × 256, a slice thickness of 700 μm was chosen, and 15 slices were collected. In addition, three-dimensional (3D) slab GE images (FLASH, TR/TE = 150/14 milliseconds, flip angle = 15°), FOV = 2.56 × 2.56 × 0.48 cm, matrix size = 128 × 96 × 24 zero-filled to 128 × 128 × 32, resulting in a spatial resolution of 200 × 200 × 150 μm^3, were collected. In some cases, the matrix size was enlarged to 256 × 128 × 64 zero-filled to 256 × 256 × 64, resulting in a spatial resolution of 100 × 100 × 75 μm^3.

Image Analysis

The MR images presented in this study are of representative rats from each group studied. The 700-μm T_2 and T_2^* comparative images were coregistered using SPM2 software (Wellcome Department of Imaging Neuroscience, University College of London) with the mutual information cost-function and trilinear algorithm for reslicing with no wrapping or image masking, such that the same slices are presented at the various time points.

Immunohistochemistry

Animals were anesthetized with chloral hydrate, and ice-cold PBS was perfused intracardially for 5 minutes, followed by 15 minutes of 4% paraformaldehyde. Brains were removed and immersed in 4% paraformaldehyde for 48 hours at 4°C and cryoprotected in 30% sucrose for another 48 hours. After immersion, the tissues were frozen at −70°C until they were cryosectioned to 10-μm axial sections. Immunohistochemistry was conducted similarly to the immunocytochemistry protocols. Mouse α-rat CD68 (ED1; 1:500∗; AbD Serotec, Raleigh, NC, http://www.ab-direct.com) was used for labeling tissue macrophages. Quantification of ED1-positive and PKH26-positive cells was performed by measuring five different fields in each section analyzed and manually counting the number of PKH26- and ED1-positive cells. The results are presented as mean ± SE. For comparing the histological appearance with the MR images, we dyed selected sections from each animal with Prussian blue stain (according to the manufacturer's instructions; Sigma-Aldrich) and found PKH26-positive cells in adjacent sections.

Statistical Analysis

The results are expressed as means ± SD, unless otherwise stated. Student's t test was used to compare two groups. Statistical calculations were performed using SPSS, version 13 (SPSS, Chicago, http://www.spss.com).

RESULTS

Characterization of NTF-Secreting MSCs

Using an immunocytochemical study, we assessed the protein expression of astrocyte and neuronal markers and neurotrophic and growth factors to test the induction protocol. We found that the induced cells had a strong positive dye for the astrocyte markers S100β, GS, and GFAP. When we quantified the percentage of cells positive for each marker, we found that S100β was found in 74.13% ± 6.50% of the treated cells compared with 24.39% ± 33.45% in the untreated group ($p < .01$), GS was positive in 54.47% ± 5.68% of the induced cells group versus 11.89% ± 8.66% of the untreated MSCs ($p < .0001$), and there was no significant change in the GFAP expression (57.26% ± 6.30% vs. 50.17% ± 13.90%). Similar to the GFAP expression, the neuronal marker β-tubulin III did not alter following induction (15.84% ± 5.09% vs. 21.03% ± 21.71%).

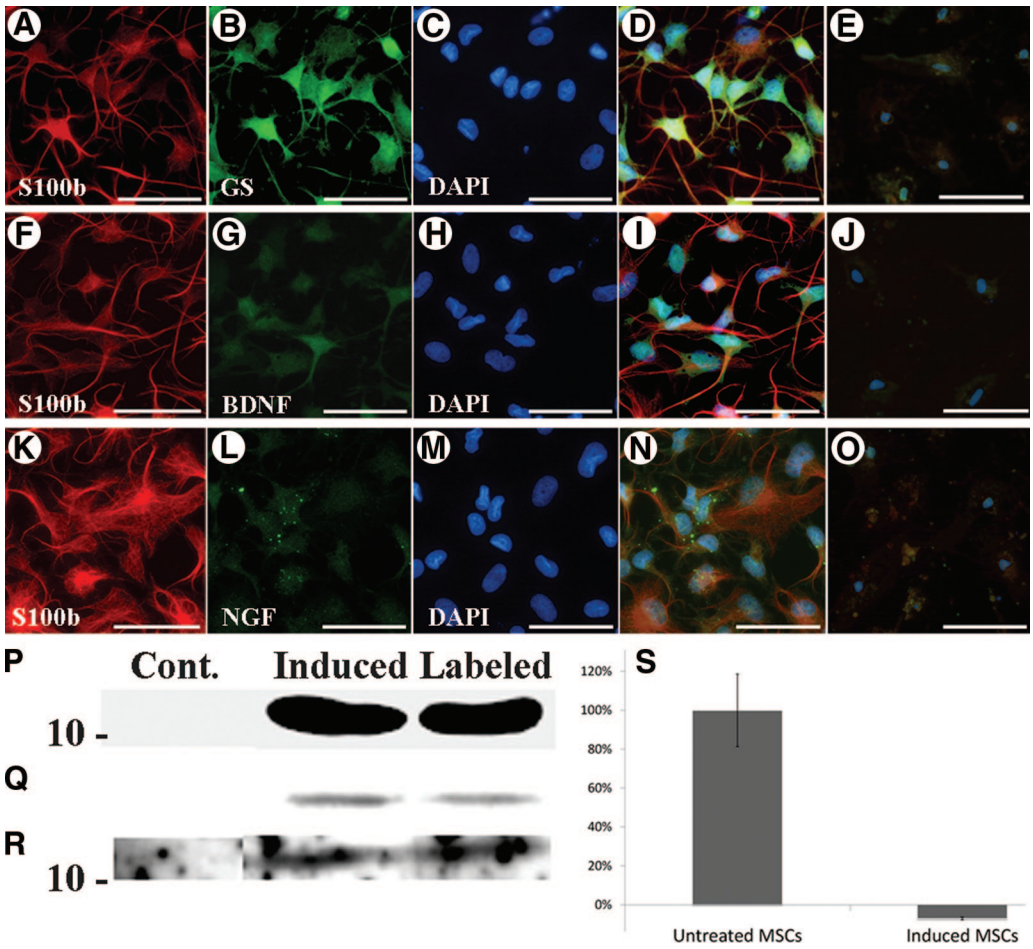

Figure 1. Differentiated MSC characterization. **(A–D):** Coexpression of GS and S100b in the induced cells. **(E):** Untreated Cont. **(F–I):** Coexpression of S100b and BDNF in the differentiated cells. **(J):** Untreated Cont. **(K–N):** Coexpression of S100b and NGF in the induced cells. **(O):** Untreated Cont. **(P):** BDNF levels measured in the media of the cells in untreated Cont. cells (serum-free medium), induced cells, and induced cells that were labeled with PKH26 and SPIOs as elaborated. **(Q, R):** The same analysis for vasculoendothelial growth factor and NGF, respectively. **(S):** 5-Bromo-2′-deoxyuridine assay for cell proliferation demonstrated a complete halt of cell proliferation on the last day of differentiation. Scale bars = 50 μm. Abbreviations: BDNF, brain-derived neurotrophic factor; Cont., control; DAPI, 4,6-diamidino-2-phenylindole dihydrochloride; GS, α-glutamine synthetase; MSC, mesenchymal stem cell; NGF, nerve growth factor; S100b, S100β.

The induced MSCs were found to be positive when dyed for BDNF (41.19% ± 13.24% postinduction compared with 6.05% ± 6.72% in the untreated group; $p < .001$), NGF (39.32% ± 7.40% vs. 8.93% ± 15.74%; $p < .01$), and VEGF (45.00% ± 5.60% vs. 4.87% ± 7.38%; $p < .0001$) but not GDNF. We also demonstrated a double stain placing the NTFs within the S100β-positive cells (Fig. 1A–1O).

The most important test for the functional result of the differentiation protocol was to prove the secretion of the neurotrophic and growth factors. Therefore, we concentrated the media of the untreated MSCs, the induced cells, and the induced cells after they were labeled with PKH26 dye and SPIO, as described above, to determine whether the labeling process altered the differentiation protocol. The presence of BDNF, NGF, VEGF, and GDNF in these media was analyzed using immunoblotting. All these factors except for GDNF were significantly increased compared with MSC controls. No differences were found between the differentiated cells and the SPIO- and PKH26-labeled differentiated cells (Fig. 1P–1R). We found markedly reduced proliferation in induced cells, in comparison with MSCs grown in the growth medium, as shown by the BrdU assay (Fig. 1S).

Migration Tracking In Vivo: MRI Study

In vivo T_2 WI of the rat brain on the day of QA and NTF-secreting MSC administration (day 0) and at 8 and 18 days post-transplantation are depicted in Figure 2. The axial and coronal images (Fig. 2) revealed an edema in the striatum extending slightly to cortical areas and the anterior parts of the thalamus on day 0 that progressed until day 3 (data not shown) and then gradually disappeared. On day 18, it was clearly visible that the damage was indeed confined mostly to the striatum.

Figure 3A–3C shows the corresponding 2D axial T_2^* WI, which are more sensitive to the magnetic field inhomogeneities that are induced by the SPIO particles in the labeled cells. On day 0, the deposition of labeled induced cells is clearly visible as a large hypointense region, posterior to the thalamus. The QA injection site exhibited a small injection mark that appeared as a small hypointense spot in the striatum. There were no additional hypointense marks in the striatum on day 0.

On days 8 and 18, two major changes in the signal from the brain were noted: the path of the NTF-secreting MSCs toward the striatum and the accumulation of these cells in various places inside it. The hypointense regions intensified on day 18, showing a marked accumulation in the striatum. The induced

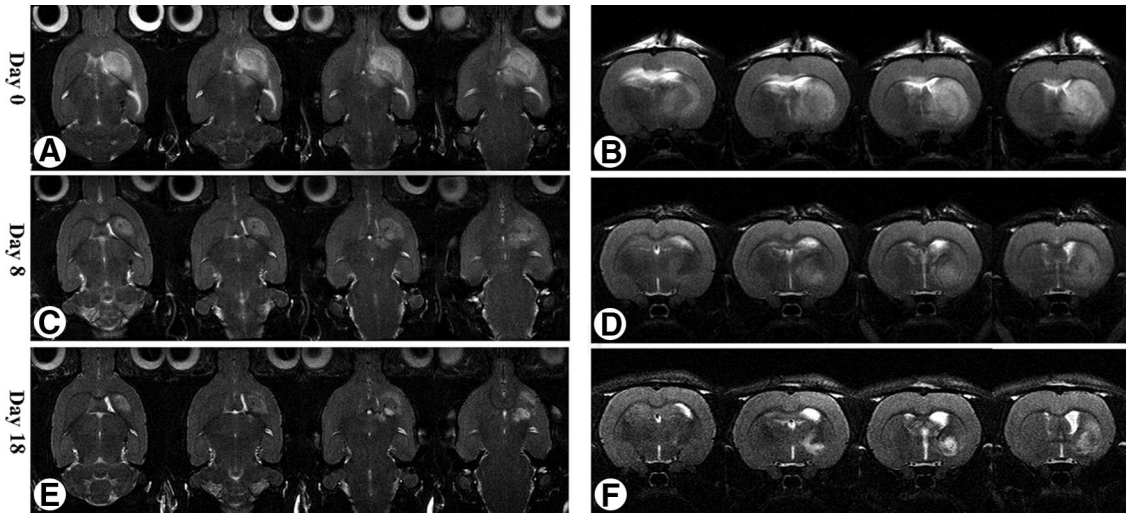

Figure 2. Time course of striatal lesion induced by quinolinic acid injection. Axial **(A, C, E)** and coronal **(B, D, F)** T_2 weighted magnetic resonance images. The initial edema subsided after 3 days (data not shown). The lesion was mainly confined to the striatum.

MSCs migrated along the internal capsule, according to an anatomical analysis [27]. The trail of the transplanted cells occurred in all three dimensions, first inferiorly, then medially and anteriorly, and finally laterally arriving at the striatum. No particular MRI section can visualize the complete trail because of the 3D nature of the movement.

To investigate the local distribution of cells in the damaged area, 3D axial gradient echo images with a resolution of $100 \times 100 \times 75\ \mu m^3$ were acquired (Fig. 3D; four slices are shown). Several sites of accumulation were obvious in these images. The accumulation of the migrating cells at the end of the pathway was clear. However, other, smaller areas where NTF-secreting MSCs accumulate were noted in the striatum. Some of these accumulation sites were found close to hyperintense regions, suggesting that, indeed, these cells gather close to areas that are more severely damaged (Fig. 3E). The pathway and the various accumulation sites were apparent in the axial spatial sequence of day 18 (supplemental online data).

In one case, accumulation of NTF-secreting cells was not confined to the striatum. Figure 4 depicts the time-course 2D axial T_2 WI of a rat suffering extensive cortical damage in addition to the striatal lesion (Fig. 4A–4C). In these images, such a marked accumulation in the cortex had occurred by day 18 that the T_2 WI provided sufficient contrast for viewing the accumulation (Fig. 4C). Indeed, the $200 \times 200 \times 150\ \mu m^3$ high-resolution 3D-GE images clearly showed that the accumulation in the cortex occurred mostly in more hyperintense areas, again suggesting that the induced MSCs can sense the areas that are probably more severely damaged (Fig. 4D, 4E). Importantly, all six rats that were treated by both QA and NTF-secreting stem cells showed migratory capabilities of the NTF-secreting cells.

Figure 5 shows the control groups of this study. The first control group consisted of animals that were injected with QA and SPIOs only, at a dose similar to the dose to which the 2.5×10^5 cells were exposed. Figure 5A shows the anatomical features and lesion in T_2 WI on day 0. Figure 5B demonstrates the effect of SPIOs on T_2^* WI on day 18. Even though the influence of the SPIOs on the signal was very large at the deposition site, no hypointense signal could be found in the striatum on days 8 (data not shown) and 18. This was also confirmed by the high-resolution 3D-GE images (Fig. 5C) collected on day 18 post-transplantation. These results were consistent for all three rats in this control group, and none showed any hypointense signals in the striatum or at any area between the SPIO deposition site and the QA lesion site except the QA injection mark.

The second control group was treated with SPIO-labeled cells and PBS (i.e., without inducing a striatal lesion). Figure 5D demonstrates the anatomical features by T_2 WI on day 0, and Figure 5E shows the T_2^* WI sensitive to the transplanted cells on day 18. Again, no hypointense signal could be found in the striatum on day 18, as the high-resolution 3D-GE images of day 18 (Fig. 5F) confirmed. These results were consistent for all three rats in this control group.

Migration Tracking: Histological Study

To coordinate the histological and imaging results, we dyed six different tissue sections (axial sections, comparable to the MRI; Fig. 6A, 6B) of three animals of the treated group with a Prussian blue stain to detect iron deposits. We found a clear correlation between the MRI hypointense signals and the Prussian blue- and PKH26-positive sites (in adjacent sections) in all the sections, at all of the sites searched (Fig. 6). We found fewer Prussian blue-positive cells than PKH26-positive cells in adjacent sections, probably as a result of asymmetric uptake of the SPIOs.

To quantify cell phagocytosis, we dyed six different sections with the macrophage marker ED1 (CD68) of the rat, with a fluorescent secondary antibody. We searched for PKH26-positive cells (the transplanted cells) that coexpress ED1, as a sign for cell phagocytosis. We located macrophages mainly in the lesion site, but also at the transplantation area and all along the migration route. This latter distribution was not found in the controls treated with SPIO alone. To assess the proportion of the phaged cells of the total surviving cells, we quantified them. We found out that only $23.07\% \pm 7.31\%$ of the surviving transplanted cells were positive for ED1 and hence phaged.

The control groups demonstrated the same high correlation to the MR images as did the group that was treated with both QA and cells (Fig. 6). Specifically, in the control group treated with QA and SPIOs without any cellular therapy, we found a Prussian blue-positive stain only around the SPIO deposition site (Fig. 6H), and not in the striatum. In the control group that was treated with cells and PBS, without QA, we found the injected cells only around the transplantation site of the cells in a radial distribution, using both the fluorescent marker and Prussian blue stain (Fig. 6J, 6K).

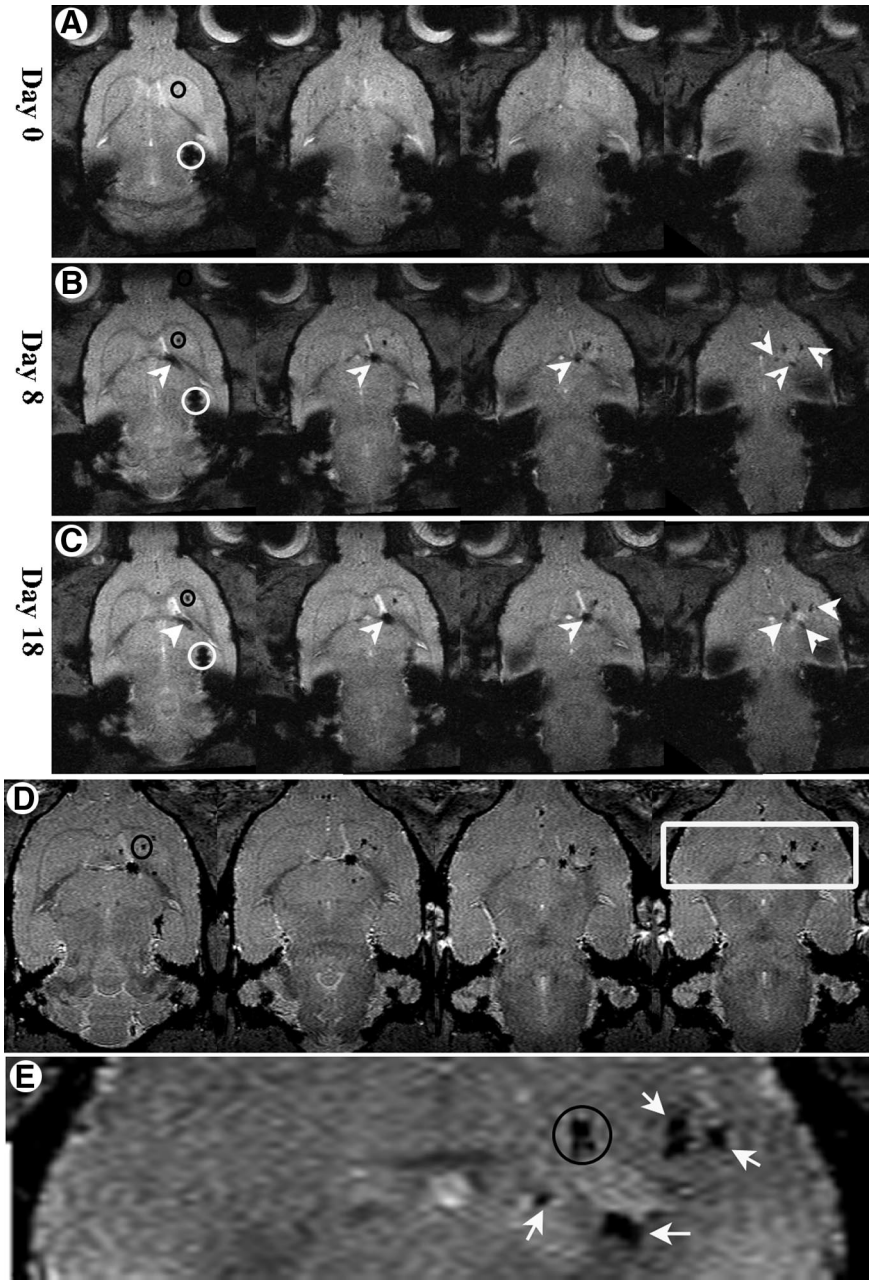

Figure 3. Migration of cells over time. **(A–C):** Axial two-dimensional T_2^* weighted images on days 0, 8, and 18 post-transplantation, respectively. **(D):** Day 18 high-resolution 100 × 100 × 75 μm^3 axial three-dimensional-gradient echo images; the slices are not contiguous. **(E):** Enlargement of box in **(D)**. Note that the accumulation can be clearly seen next to hyperintense regions in the image, suggesting that the cells accumulated adjacent to more severely damaged regions. Black circles represent the quinolinic acid (QA) injection mark (shown only on one slice of each time point for convenience; the QA injection mark can be seen in all slices). White circles depict the stem cell transplantation site. White arrows and arrowheads depict the pathway and accumulation sites of the stem cells.

DISCUSSION

In this paper, we have described a protocol for inducing rat bone-marrow-derived MSCs into NTF-secreting cells. We have also demonstrated the migratory capabilities of these cells toward a QA-induced lesion, applying two different and reciprocal modalities: the in vivo tracking of the cells by MRI and the histological study with two separate markers.

MSCs hold a promising future for neurodegenerative disease therapy [29, 30]. Whether MSCs can differentiate into nonmesodermal cells and tissues remains controversial [30]. Normally, mature stem cells are supposed to be committed to their lineage. However, several recent reports have shown the differentiation capabilities of MSCs toward the neural lineages under specific medium conditions [31–37]. Our group has previously shown [6], as have others [38, 39], that MSCs basally express several neural markers and NTFs. We have also shown that under specific conditions, MSCs can differentiate into dopamine-producing cells that express neuronal markers [40–42].

As cited, most of the earlier studies have tried to differentiate MSCs into neuronal cells, as part of the cell replacement strategy. Glia and astrocytes are responsible for tissue support, and more importantly in this nexus, astrocytes produce and secrete NTFs, thus becoming promising candidates for the tissue protection strategy. For this purpose, we developed a novel two-step protocol that induces MSCs toward the NTF-secreting astroglial lineage as opposed to the neuronal lineage. The induction protocol included growth factors known to induce neural differentiation in MSCs, such as epidermal growth factor, basic fibroblast growth factor, and PDGF [33, 43], and N2

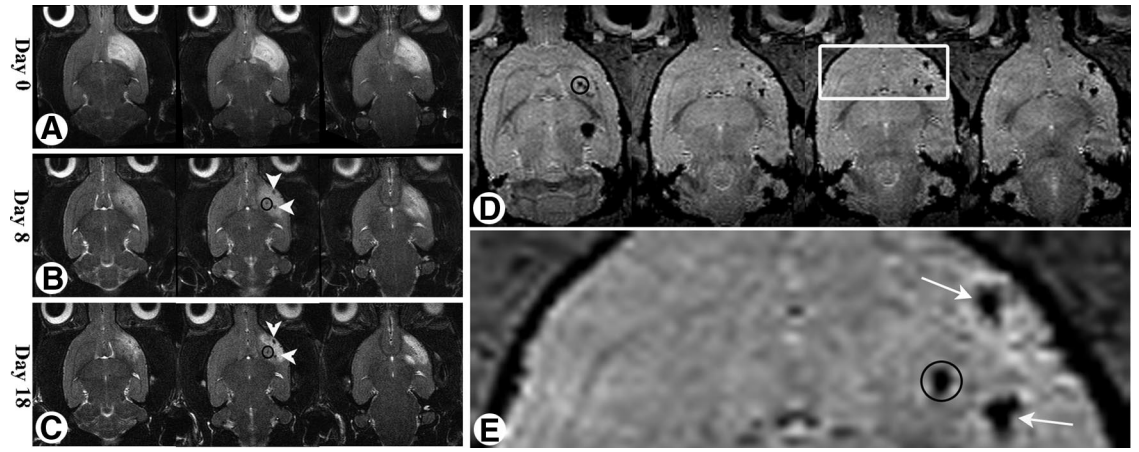

Figure 4. Induced mesenchymal stem cells (MSCs) migrate toward a cortical lesion. **(A–C):** Time-course axial T_2 weighted images of the rat that suffered a cortical damage. **(D):** Axial three-dimensional-gradient echo high-resolution $200 \times 200 \times 150$ μm^3 images clearly showing accumulation of MSCs in the cortex as well as the striatum. **(E):** Enlargement of box in **(D)**. The observation that cells accumulate in hyperintense regions was independent of the area of damage, thus indicating the homing capabilities of the cells. The hypointense signals rise from the presence of viable stem cells. Black circles represent the quinolinic acid (QA) injection mark (shown only on one slice of each time point for convenience; the QA injection mark can be seen in all slices). White arrows and arrowheads depict the accumulation sites of the stem cells.

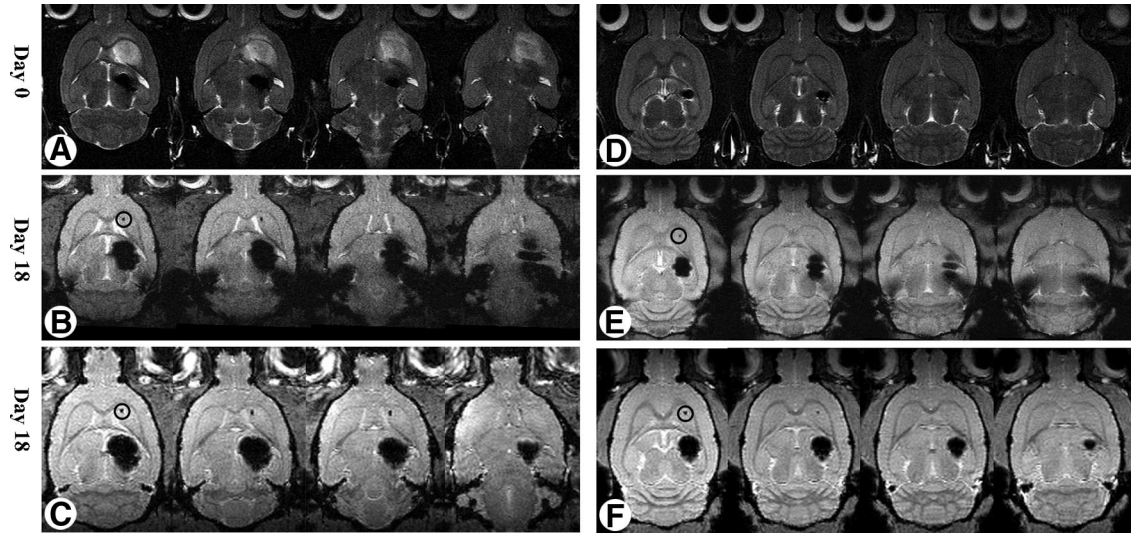

Figure 5. Control groups. **(A–C):** Control group treated with quinolinic acid (QA) and superparamagnetic iron oxide (SPIO) only. **(A):** Axial T_2 weighted images (WI) from day 0 showing the same striatal lesion as in the induced mesenchymal stem cell (MSC)-transplanted animals. **(B):** Day 18 T_2^* WI showing no accumulation of SPIOs at the lesion site. **(C):** High-resolution $200 \times 200 \times 150$ μm^3 three-dimensional (3D)-gradient echo (GE) images from day 18 demonstrate the lack of SPIOs accumulation in the striatum. This indicates that the cells did not leak to the lower parts of the brain. **(D–F):** Control group treated with NTF-secreting MSCs and phosphate-buffered saline. **(D):** Axial T_2 WI of day 0 exhibits the deposition site and shows no lesion in the striatum. **(E):** Day 18 T_2^* WI showing no migration pathway and no accumulation of cells at the striatum. **(F):** High-resolution $200 \times 200 \times 150$ μm^3 3D-GE images from day 18 show that the striatum is indeed free of NTF-secreting MSCs, indicating that the cells have no bias toward the unimpaired striatum. Black circles represent the QA injection mark (shown only on one slice of each time point for convenience; the QA injection mark can be seen in all slices).

cocktail, which is reported to have increased survival of neural primary cultures and differentiation [44]. Cyclic AMP, an important intracellular secondary messenger, is also linked to this process [39, 45]. We excluded retinoic acid, a substance that we previously used for neuronal differentiation and not astroglial differentiation. Using our distinct protocol, cells expressed several neural markers, mainly astrocytic (GS, S100β) and, to a certain extent, neuronal markers as well, since S100β, which is considered an astrocytic marker, can be found in distinct neuronal populations [46]. The process of differentiation induced a significantly larger production of certain NTFs, such as BDNF, NGF, and VEGF, compared with untreated cells. Furthermore, we demonstrated that the expression of NTFs was colocalized with the expression of S100β. More importantly, we showed that not only do the cells produce NTFs, as seen by immunostaining, but they also secrete them, as shown by a Western blot analysis of the conditioned cell media.

Another issue in the field of stem cells is tumorigenesis of cells, particularly embryonic and fetal-derived stem cells [47]. Therefore, we examined the proliferation rate of the cells postinduction and revealed that our differentiation protocol inhibits proliferation, as indicated by the BrdU proliferation assay. This result is important in the context of our study, as a recent article has shown that proliferation of stem cells in vivo induces SPIO dilution in prelabeled cells along the migratory route [48]. We have also shown that labeling the cells with SPIO and PKH26 does not alter the NTF secretion postinduction. This is not

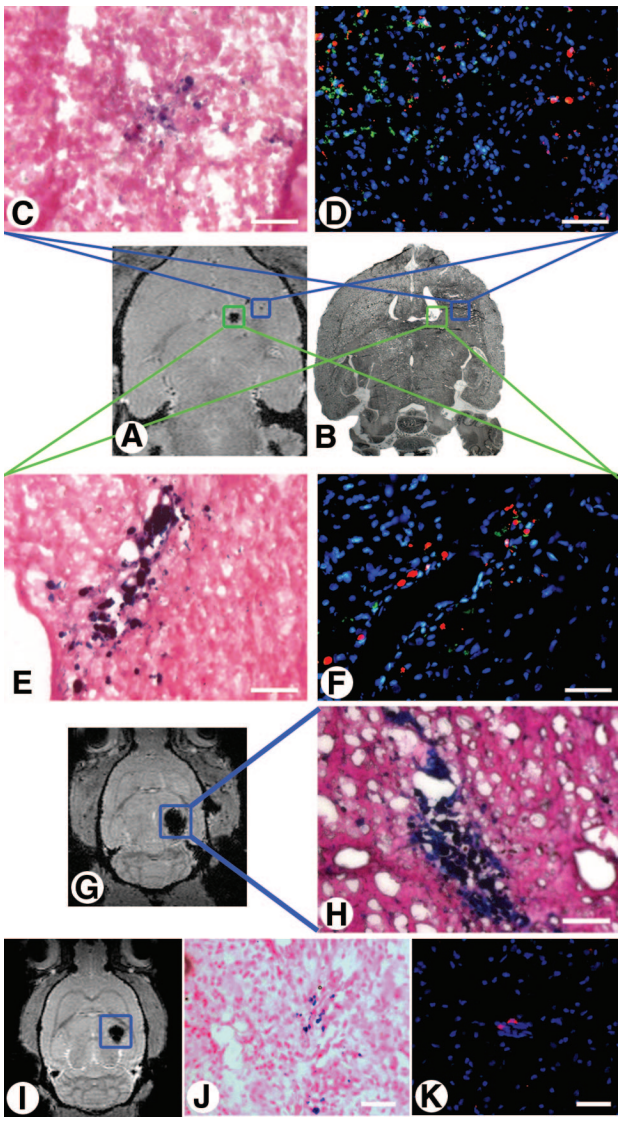

Figure 6. Histology corroborated the magnetic resonance imaging (MRI) images. **(A):** One slice of high-resolution 100 × 100 × 75 μm^3 three-dimensional-gradient echo images on day 18 from the NTF-secreting cells and quinolinic acid (QA)-treated group. **(B):** The matching histology section. Two representative hypointense areas that can be seen in the MRI slice were analyzed. We found, concomitantly, both Prussian blue-positive cells **(C, E)** and PKH26-positive cells **([D, F]**, in red, in adjacent histological sections). ED1 staining **([D, F]**, in green) revealed that only partial phagocytosis had occurred. **(G, H):** A representative slice from the control group treated with superparamagnetic iron oxides without cellular treatment **(G)** and the corresponding area of the hypointense signal **(H)** in a histological section dyed with Prussian blue. **(I–K):** One representative slice from the control group treated with cells without QA **(I)** and the corresponding adjacent histological sections dyed with Prussian blue **(J)** and PKH26 with 4,6-diamidino-2-phenylindole dihydrochloride **(K)**. Scale bars = 50 μm.

trivial, since a previous study showed that SPIO labeling of MSCs inhibited chondrogenic differentiation [49].

One of the major caveats of stem cell transplantations is the fate of the transplanted cells. In the imaging field, it is difficult to delineate implanted cells from host tissue without contrast agents or markers. In a recent study, optical imaging with luciferase expression has been used to prove the migration of neural stem cells in the QA model of HD [1, 44]. Other studies have tried to delineate cells with different relaxation mechanisms in MRI, using gadolinium-based contrast agents that accumulate in the grafts because of a blood-brain barrier compromise [50]. In our study, we circumvented the low sensitivity of MRI by labeling stem cells with SPIOs and transplanting them far from the lesion. Thus, we could demonstrate cell viability, albeit indirectly. The MR images have provided a clear-cut case regarding the migration and clearly showed the path of migration, from the site of deposition to the lesion, in an 18-day course. Several accumulation sites of cells were exhibited in the lesion site. The histology findings correlated the hypointense spots to the presence of MSCs along the pathway and in the accumulation sites. In these cases, the correlation was so powerful that the histology failed to detect PKH26-labeled cells in brain areas that were not hypointense in the MR images. It is further implied that the differentiated MSCs are capable of navigating themselves to the areas that have been most severely impaired, as seen in the high-resolution T_2^* WI. This concept has been shown for stem cells in stroke models, where there is extensive damage to the brain [16, 26, 51]. In the present study, we have shown that our induced NTF-secreting MSCs reacted to a much smaller lesion, proving that not only did the cells survive the implant but they were able to sense the smaller chemotactic signal gradient.

In this study, it was imperative to show that the migration was not caused by leaking of the injected volume or by inherent affinity of the NTF-secreting MSCs toward the striatum. By using two control groups, we were able to demonstrate that it is improbable that the cells arrived at the striatum and accumulated there merely by a leaking effect, as no pathway or accumulation could be detected in any of our control animals that were treated with QA and SPIOs only. Furthermore, it seems that the cells do not have any inherent bias toward migrating to the striatum, as all of our control animals that were treated with cells and PBS (but not QA) did not exhibit migratory properties. Moreover, the cells guided themselves toward a cortical lesion in one animal. The results were consistent; that is, all of the animals treated with QA and NTF-secreting MSCs exhibited migration properties ($n = 6$), whereas all of our controls ($n = 6$) failed to show migration pathways or accumulation sites.

Our dual labeling scheme, targeted for validating the MRI study, has also offered a better opportunity to visualize the cells in histology, as colocalization was possible. Using both stains, we validated the location of the cells as the MRI had predicted. Several dozen cells were found to be positive for iron dye in a given accumulation site. As cited, there were more PKH26-positive cells than Prussian blue-labeled cells, probably because of the low dosage of SPIO labeling or, perhaps, the asymmetric uptake of the cells.

The reaction of the innate immune system to the cells, despite the allogenic transplantation, has also been tested. Previous studies showed that this could pose a problem and demonstrated up to 100% phagocytosis of the transplanted MSCs, injected into a myocardial infarct scar [52]. Moreover, a recent study has claimed that rat-derived MSCs cannot survive more than 14 days, even in a naïve rat brain [53]. In our study, we dyed the sections for the macrophage marker ED1 and proved that only a minority of the cells had been actually attacked by the immune system after 18 days. However, although MSCs are known to induce immunosuppression on their surroundings [10, 54], the cells definitely induced the immune response since ED1-positive aggregations were witnessed all along the migration path from the transplantation spot (data not shown). This was not found in SPIO-only-injected control animals.

CONCLUSION

We have presented a novel protocol that induced MSCs into NTFs secreting cell. In this study, we have used high resolution MRI to demonstrate that our NTF-secreting MSCs migrated towards the QA lesion in vivo in a rat model of HD, indirectly demonstrating the viability of the cells over a period of at least 19 days. The SPIO labeled cells corresponded very well with the histology-based study. From the therapeutic point of view, these findings are very promising, as they suggest that our differentiated MSC implants do not have to be delivered directly to the impaired sites, but can find their way toward the injury site. It is important to note that transplanting exogenous stem cells in a wounded environment poses an a priori threat to their survival. Therefore, a strategy of depositing the cells in areas that are not impaired may increase the therapeutic potential of the stem cells. In a complex microenvironment such as brain tissue, this means that MSCs will migrate from the (safe) site of deposition to the locations where they are most needed and exert their positive effect there. Future experiments will examine the efficacy of the NTF-secreting cells in the QA model of HD.

ACKNOWLEDGMENTS

The MRI scanner used in this study was purchased with grants from The Israel Science Foundation and the Raymond and Beverly Sackler Institute of Biophysics of Tel Aviv University. We thank the Alfredo Federico Strauss Center for Computational NeuroImaging of Tel Aviv University.

DISCLOSURE OF POTENTIAL CONFLICTS OF INTEREST

The authors indicate no potential conflicts of interest.

REFERENCES

1 Pineda JR, Rubio N, Akerud P et al. Neuroprotection by GDNF-secreting stem cells in a Huntington's disease model: Optical neuroimage tracking of brain-grafted cells. Gene Ther 2007;14:118–128.
2 Guidetti P, Luthi-Carter RE, Augood SJ et al. Neostriatal and cortical quinolinate levels are increased in early grade Huntington's disease. Neurobiol Dis 2004;17:455–461.
3 Guidetti P, Bates GP, Graham RK et al. Elevated brain 3-hydroxykynurenine and quinolinate levels in Huntington disease mice. Neurobiol Dis 2006;23:190–197.
4 Beal MF, Kowall NW, Ellison DW et al. Replication of the neurochemical characteristics of Huntington's disease by quinolinic acid. Nature 1986;321:168–171.
5 Pittenger MF, Mackay AM, Beck SC et al. Multilineage potential of adult human mesenchymal stem cells. Science 1999;284:143–147.
6 Blondheim NR, Levy YS, Ben-Zur T et al. Human mesenchymal stem cells express neural genes, suggesting a neural predisposition. Stem Cells Dev 2006;15:141–164.
7 Hellmann MA, Panet H, Barhum Y et al. Increased survival and migration of engrafted mesenchymal bone marrow stem cells in 6-hydroxydopamine-lesioned rodents. Neurosci Lett 2006;395:124–128.
8 Karussis D, Kassis I, Basan GS et al. Immunomodulation and neuroprotection with mesenchymal bone marrow stem cells (MSCs): A proposed treatment for multiple sclerosis and other neuroimmunological/neurodegenerative diseases. J Neurol Sci 2008;265:131–135.
9 Tang Y, Yasuhara T, Hara K et al. Transplantation of bone marrow-derived stem cells: A promising therapy for stroke. Cell Transplant 2007;16:159–169.
10 Le Blanc K, Ringden O. Immunomodulation by mesenchymal stem cells and clinical experience. J Intern Med 2007;262:509–525.
11 Chamberlain G, Fox J, Ashton B et al. Concise review: Mesenchymal stem cells: Their phenotype, differentiation capacity, immunological features, and potential for homing. STEM CELLS 2007;25:2739–2749.
12 Syková E, Jendelova P. Migration, fate and in vivo imaging of adult stem cells in the CNS. Cell Death Differ 2007;14:1336–1342.
13 Magnitsky S, Walton RM, Wolfe JH et al. Magnetic resonance imaging as a tool for monitoring stem cell migration. Neurodegener Dis 2007;4:314–321.
14 Guzman R, Uchida N, Bliss TM et al. Long-term monitoring of transplanted human neural stem cells in developmental and pathological contexts with MRI. Proc Natl Acad Sci U S A 2007;104:10211–10216.
15 Bulte JW, Kraitchman DL. Iron oxide MR contrast agents for molecular and cellular imaging. NMR Biomed 2004;17:484–499.
16 Modo M, Mellodew K, Cash D et al. Mapping transplanted stem cell migration after a stroke: A serial, in vivo magnetic resonance imaging study. Neuroimage 2004;21:311–317.
17 Heyn C, Bowen CV, Rutt BK et al. Detection threshold of single SPIO-labeled cells with FIESTA. Magn Reson Med 2005;53:312–320.
18 Shapiro EM, Sharer K, Skrtic S et al. In vivo detection of single cells by MRI. Magn Reson Med 2006;55:242–249.
19 Tran PB, Ren D, Veldhouse TJ et al. Chemokine receptors are expressed widely by embryonic and adult neural progenitor cells. J Neurosci Res 2004;76:20–34.
20 Curtis MA, Faull RL, Eriksson PS. The effect of neurodegenerative diseases on the subventricular zone. Nat Rev Neurosci 2007;8:712–723.
21 Tattersfield AS, Croon RJ, Liu YW et al. Neurogenesis in the striatum of the quinolinic acid lesion model of Huntington's disease. Neuroscience 2004;127:319–332.
22 Gordon RJ, Tattersfield AS, Vazey EM et al. Temporal profile of subventricular zone progenitor cell migration following quinolinic acid-induced striatal cell loss. Neuroscience 2007;146:1704–1718.
23 Henry RA, Hughes SM, Connor B. AAV-mediated delivery of BDNF augments neurogenesis in the normal and quinolinic acid-lesioned adult rat brain. Eur J Neurosci 2007;25:3513–3525.
24 Carpentino JE, Hartman NW, Grabel LB et al. Region-specific differentiation of embryonic stem cell-derived neural progenitor transplants into the adult mouse hippocampus following seizures. J Neurosci Res 2008;86:512–524.
25 Lee ST, Park JE, Lee K et al. Noninvasive method of immortalized neural stem-like cell transplantation in an experimental model of Huntington's disease. J Neurosci Methods 2006;152:250–254.
26 Hoehn M, Kustermann E, Blunk J et al. Monitoring of implanted stem cell migration in vivo: A highly resolved in vivo magnetic resonance imaging investigation of experimental stroke in rat. Proc Natl Acad Sci U S A 2002;99:16267–16272.
27 Paxinos G, Watson C. The Rat Brain. 4th ed. San Diego: Academic Press, 1998.
28 Frank JA, Miller BR, Arbab AS et al. Clinically applicable labeling of mammalian and stem cells by combining superparamagnetic iron oxides and transfection agents. Radiology 2003;228:480–487.
29 Kan I, Melamed E, Offen D. Autotransplantation of bone marrow-derived stem cells as a therapy for neurodegenerative diseases. Handb Exp Pharmacol 2007;180:219–242.
30 Krabbe C, Zimmer J, Meyer M. Neural transdifferentiation of mesenchymal stem cells-a critical review. APMIS 2005;113:831–844.
31 Lei Z, Yongda L, Jun M et al. Culture and neural differentiation of rat bone marrow mesenchymal stem cells in vitro. Cell Biol Int 2007;31:916–923.
32 Wang TT, Tio M, Lee W et al. Neural differentiation of mesenchymal-like stem cells from cord blood is mediated by PKA. Biochem Biophys Res Commun 2007;357:1021–1027.
33 Kim S, Honmou O, Kato K et al. Neural differentiation potential of peripheral blood- and bone-marrow-derived precursor cells. Brain Res 2006;1123:27–33.
34 Krampera M, Marconi S, Pasini A et al. Induction of neural-like differentiation in human mesenchymal stem cells derived from bone marrow, fat, spleen and thymus. Bone 2007;40:382–390.
35 Mareschi K, Novara M, Rustichelli D et al. Neural differentiation of human mesenchymal stem cells: Evidence for expression of neural markers and eag K+ channel types. Exp Hematol 2006;34:1563–1572.
36 Zemchikhina VN, Golubeva ON. The capacity of mesenchymal stem cells for neural differentiation in vitro. Tsitologiia 2005;47:644–648.
37 Long X, Olszewski M, Huang W et al. Neural cell differentiation in vitro from adult human bone marrow mesenchymal stem cells. Stem Cells Dev 2005;14:65–69.
38 Arnhold S, Klein H, Klinz FJ et al. Human bone marrow stroma cells display certain neural characteristics and integrate in the subventricular

compartment after injection into the liquor system. Eur J Cell Biol 2006;85:551–565.
39 Deng J, Petersen BE, Steindler DA et al. Mesenchymal stem cells spontaneously express neural proteins in culture and are neurogenic after transplantation. STEM CELLS 2006;24:1054–1064.
40 Levy YS, Merims D, Panet H et al. Induction of neuron-specific enolase promoter and neuronal markers in differentiated mouse bone marrow stromal cells. J Mol Neurosci 2003;21:121–132.
41 Kan I, Ben-Zur T, Barhum Y et al. Dopaminergic differentiation of human mesenchymal stem cells—Utilization of bioassay for tyrosine hydroxylase expression. Neurosci Lett 2007;419:28–33.
42 Barzilay R, Kan I, Ben-Zur T et al. Induction of human mesenchymal stem cells into dopamine-producing cells with different differentiation protocols. Stem Cells Dev 2008;17:547–554.
43 Li Q, Hosaka N, Cui W et al. Lin(-)CD34(-) bone marrow cells from adult mice can differentiate into neural-like cells. Neurosci Lett 2006; 408:51–56.
44 Bottenstein JE. Growth of neural cells in defined media. In: Bottenstein JE, Gordon S, eds. Cell Culture in the Neuroscience: Current Topics in Neurobiology. New York: Plenum Press, 1985:1–40.
45 Chu MS, Chang CF, Yang CC et al. Signalling pathway in the induction of neurite outgrowth in human mesenchymal stem cells. Cell Signal 2006;18:519–530.
46 Rickmann M, Wolff JR. S100 protein expression in subpopulations of neurons of rat brain. Neuroscience 1995;67:977–991.
47 Master Z, McLeod M, Mendez I. Benefits, risks and ethical considerations in translation of stem cell research to clinical applications in Parkinson's disease. J Med Ethics 2007;33:169–173.
48 Walczak P, Kedziorek DA, Gilad AA et al. Applicability and limitations of MR tracking of neural stem cells with asymmetric cell division and rapid turnover: The case of the shiverer dysmyelinated mouse brain. Magn Reson Med 2007;58:261–269.
49 Kostura L, Kraitchman DL, Mackay AM et al. Feridex labeling of mesenchymal stem cells inhibits chondrogenesis but not adipogenesis or osteogenesis. NMR Biomed 2004;17:513–517.
50 Guzman R, Meyer M, Lovblad KO et al. Striatal grafts in a rat model of Huntington's disease: Time course comparison of MRI and histology. Exp Neurol 1999;156:180–190.
51 Rice HE, Hsu EW, Sheng H et al. Superparamagnetic iron oxide labeling and transplantation of adipose-derived stem cells in middle cerebral artery occlusion-injured mice. AJR Am J Roentgenol 2007;188:1101–1108.
52 Amsalem Y, Mardor Y, Feinberg MS et al. Iron-oxide labeling and outcome of transplanted mesenchymal stem cells in the infarcted myocardium. Circulation 2007;116:I38–I45.
53 Coyne TM, Marcus AJ, Woodbury D et al. Marrow stromal cells transplanted to the adult brain are rejected by an inflammatory response and transfer donor labels to host neurons and glia. STEM CELLS 2006;24: 2483–2492.
54 Xu G, Zhang L, Ren G et al. Immunosuppressive properties of cloned bone marrow mesenchymal stem cells. Cell Res 2007;17:240–248.


See www.StemCells.com for supplemental material available online.